A template bank to search for gravitational waves from inspiralling compact binaries: II. Phenomenological model

T. Cokelaer[1]

[1]*School of Physics and Astronomy, Cardiff University, Cardiff CF24 3AA, UK*

We describe the phenomenological template bank that was used to search for gravitational waves from non-spinning black hole binaries in the second, third and fourth LIGO science runs. We briefly explain the design of the bank, whose templates are based on a phenomenological detection template family. We show that this template bank gives matches greater than 95% with the physical template families that are expected to be captured by the phenomenological templates.

PACS numbers:

I. MOTIVATION

The Laser Interferometer Gravitational-Wave Observatory (LIGO) detectors [1] have reached their design sensitivity curves. The fifth science run (S5) began in November 2005 and should be completed by September 2007, with the goal of acquiring a year's worth of data in coincidence between the three LIGO interferometers. Each successive LIGO science run has witnessed improvement from both experimental and data analyst's point of view. On the experimental side, better stationarity of the data and detector sensitivities closer to design sensitivity curve were achieved. On the data analysis side, search pipeline was tuned and new techniques were developed to reduce the background rate while keeping detection efficiencies high.

Among the sources of gravitational waves that ground-based detectors are sensitive to, inspiralling compact binaries are among the most promising. Several searches for inspiralling compact binaries in the LIGO data have been pursued: primordial black holes (PBH) [2, 3], binary neutron stars (BNS) [3–5], and intermediate mass binary black holes (BBH) [3, 6]. In this paper, we focus on the BBH search, which is the most peculiar. Indeed, even though heavier BBH systems are accessible each time the detector sensitivity improves in the low frequency range, BBH waveforms remain short in the LIGO band. During the second science run (S2) [6], the lower cut-off frequency was set to 100 Hz, which restricted the total mass of the search to be below 40 $M_{\odot}$, and the longest expected signal was about 0.60 s long.

Matched filtering is commonly used to search for gravitational wave signals emitted by inspiralling compact binaries. This method is appropriate for the search of light systems such as PBH and BNS, and lightest BBH systems for which accurate waveforms are available. In the case of heaviest systems (e.g., BBH), post-Newtonian (PN) expansion [7] begins to fail as the characteristic velocity v/c is not close to zero anymore (e.g., see [8]). There is a wide variety of techniques that allow to describe the gravitational flux and energy generated during the late stage of the inspiralling phase (e.g., see [7, 8]). However, they lead to various physical template families, and overlaps between them are not necessarily high, especially in the BBH case where the last orbits significantly contribute to the final signal-to-noise ratio (SNR). Therefore, if we search for BBH using only one of the approximations it might lead to loss of events, and one solution would be to carry out a matched filtered search deploying all the known waveform families.

Instead of searching for BBH signals using several physical template families, a single *detection template family*(DTF) was proposed by Buonanno, Chen, and Vallisneri [8] (BCV) with the goal of embedding the different physical approximations all into a single phenomenological model. This detection template family is known as BCV template family and has been used to search for non-spinning BBH signals in LIGO data [3, 6].

In this paper, we describe the BCV template bank that was developed and used to search for BBH signals in the second (S2), third (S3), and fourth (S4) LIGO science runs [3, 6]. In Sec. II, we briefly discuss the template parameters and the filtering process related to BCV templates. In Sec. III, we describe the BCV template bank, and the parameters that define the spacing between templates. In Sec. IV, we test and validate the proposed template bank with exhaustive simulated injections. Finally, in Sec. V, we summarize the results.

II. THE BCV TEMPLATE FAMILY

The detection template family that was proposed in [8] is built directly from the Fourier transform [9] of GW signals by writing the amplitude and phase as polynomials in the gravitational wave frequency law that appear in the stationary phase approximation [10]. In the frequency domain, the BCV templates are defined to be

$$h\left(f\right) = \mathcal{A}(f) e^{i\psi(f)}\,, \tag{2.1}$$

where

$$\mathcal{A}(f) \;=\; f^{-7/6}\left(1-\alpha f^{2/3}\right)\theta\left(f_{\rm cut}-f\right), \tag{2.2}$$

$$\psi(f) \;=\; 2\pi f t_0 + \phi_0 + f^{-5/3}\sum_{k=0}^{N}\psi_k f^{k/3}\,. \tag{2.3}$$

The parameter α is a shape parameter introduced to capture post-Newtonian amplitude corrections. Because var-

ious models predict different terminating frequencies, an ending cut-off frequency $f_{\rm cut}$ is introduced. In the amplitude expression, the waveform is multiply by a Heaviside step function, $\theta\left(f_{\rm cut}-f\right)$. In the right hand side of equation 2.3, we use only two parameters ψ_0 and ψ_3, which suffices to obtain a high match with most of the PN models [8]. The symbol ψ_3 here is the same as the symbol $\psi_{3/2}$ in [8].

The ψ_k parameters are the phase parameters of the phenomenological waveform, which cannot be directly linked to the physical mass parameters; the BCV templates are made for detection, not for parameter estimation. Nevertheless, a good approximation (for low masses) of the chirp mass $\mathcal{M}$ is given by

$$\psi_0 \approx \frac{3}{128}\left(\frac{1}{\pi\mathcal{M}}\right)^{5/3} . \tag{2.4}$$

In Sec. IV D, we investigate the range of validity of this relation.

The filtering of a data set using BCV templates is not as trivial as the one that uses physical template families. Indeed, the BCV filtering implies a search in six dimensions (ψ_0, ψ_3, α, ϕ_0, t_0, and $f_{\rm cut}$). Hopefully, the SNR can be analytically maximized over α, ϕ_0 and t_0, which reduces the search to three dimensions only. The maximization over t_0 is straightforward (inverse Fourier transform), but the maximization over α and ϕ_0 is not. In order to perform the filtering and the maximization over α and ϕ_0, we need to construct orthonormal basis vectors $\left\{\hat{h}_k\right\}_{k=1,..,4}$ for the 4-dimensional linear subspace of templates with $\phi_0 \in [0, 2\pi[$ and $\alpha \in (-\infty, \infty)$, and we want the basis vectors to satisfy $\left\langle \hat{h}_i, \hat{h}_j \right\rangle = \delta_{ij}$ (see the Appendix for details). The SNR before maximization is given by

$$\begin{aligned} \rho &= x_1 \cos\omega \cos\phi_0 + x_2 \sin\omega \cos\phi_0 \\ &+ x_3 \cos\omega \sin\phi_0 + x_1 \sin\omega \sin\phi_0 \,, \end{aligned} \tag{2.5}$$

where $x_i = \left\langle s, \hat{h}_i \right\rangle$, and s is the data to be filtered [1]. The parameter ω is a function of α (see equation B7).

The SNR ρ can be maximized over ϕ_0 and $\omega(\alpha)$. In [6], the maximization is done over the two new parameters $A = \omega + \phi_0$ and $B = \omega - \phi_0$. The maximized SNR (independent of α and ϕ_0), is denoted ρ_U, and is given by

$$\rho_U = \frac{1}{\sqrt{2}}\left(\sqrt{V_0 + \sqrt{V_1^2 + V_2^2}}\right) , \tag{2.6}$$

where V_k are function of x_i (see Appendix for details).

[1] The expression of the SNR shows that the expected rate of false alarm follows a chi-square distribution with 4 degrees of freedom instead of 2 in the case of physical template families

The SNR provided in equation 2.6 is the *unconstrained* SNR that is independent of any constraint on the range of the parameter $\alpha_F = \alpha f^{2/3}$. Yet, in [8], the authors suggested that the parameter α_F should be restricted to the range $[0, 1]$. Indeed when $\alpha_F > 1$, the amplitude in equation 2.2 becomes negative, which corresponds to unphysical waveforms. Moreover, when $\alpha_F < 0$, the amplitude factor can substantially deviate from the predictions of PN theory.

In S2 [6], many accidental triggers were found with $\alpha_F > 1$, and the calculation of the SNR was unconstrained (as in equation 2.6) leading to high false alarm rate, which was decreased, a posteriori, by removing all triggers for which $\alpha_F > 1$ (without decreasing the detection efficiency). Nevertheless, triggers that verified $\alpha_F < 0$ were kept because the false alarm rate did not decrease significantly when this selection was applied.

In S3 and S4, the search for BBH systems deployed a filtering that takes α_F value into account, by using a maximization of equation 2.5 that leads to a *constrained* SNR denoted ρ_C. The expression for the constrained SNR depends now on the value of α_F: if $0 \leq \alpha_F \leq 1$, then no constraint is applied (i.e., $\rho_C = \rho_U$). However, if $\alpha_F > 1$ or $\alpha_F < 0$, then a constrained SNR is used so that the final α_F parameter is either 0 or 1. When the SNR is constrained then $\rho_C \leq \rho_U$. The expressions of the constrained SNR are provided in the Appendix.

It is worth noticing that for the study that follows, we always use a constrained SNR but using an unconstrained SNR should not significantly change the results of our simulations and/or template bank placement. Indeed, simulated injections are generated with physical template families for which we do not expect α_F to be unphysical (i.e., outside $[0-1]$), as we shall see in Sec. V. Using a constrained SNR has an important impact when dealing with real analysis, where most of the accidental triggers have α_F between $(-\infty\,, \infty)$ (and therefore in $(-\infty\,, 0[\cup]1\,, \infty)$ as well, where $\rho_C < \rho_U$). Consequently, in general, for a given threshold λ, the SNR of accidental triggers have $\rho_C < \rho_U$, and the rate is therefore lower with respect to a search with unconstrained SNR. The number of triggers that needs to be stored is lower by an order of magnitude. Nevertheless, the final rate of triggers between the two methods may be equivalent because of *a posteriori* cuts on α_F when an unconstrained SNR is used as in [6].

III. BCV TEMPLATE BANK DESIGN

Template bank placement has been investigated in several papers [11–16] in the context of physical template families. We refer the reader to the established literature in this subject area.

A. Metric Computation in ψ_0–ψ_3 Plane

In the case of BCV templates, the mismatch metric g_{ij} [12] is known (see Appendix), and is constant over the entire ψ_0–ψ_3 parameter space. Nonetheless, the metric components are strongly related to the lower cut-off frequency of the search, which affects the moments used to calculate the metric (see equation A6). The moment computation also depends on the α parameter, as discussed later. For now, let us suppose that the moments are fixed.

Because the metric is constant, the placement of templates on the ψ_0–ψ_3 parameter space is straightforward. In the first search for BBH signals [6], the template placement used a square lattice, and templates were placed parallel to the ψ_0 axes. In S3 and S4 BBH searches, an optimal placement was used (hexagonal lattice), which reduced the requested computing ressources (and trigger rate) by 30% with respect to S2. In this paper, we only consider tests related to the hexagonal lattice case. In S3 and S4 BBH searches, we placed the templates parallel to the first eigenvector rather than parallel to the ψ_0 axis.

The target waveforms are BBH systems for which the lowest component mass is set to 3 $M_\odot$ and the highest component mass is defined by the detector lower cut-off frequency (up to 80 $M_\odot$ in S4). Simulations show that to detect such target waveforms, the range of phenomenological parameters should be set to $\psi_0 \in [10000,\ 550000]$ Hz$^{5/3}$ and $\psi_3 \in [-5000,\ -10]$ Hz$^{2/3}$. As explained in Sec. III D, if we search for BBH systems only, a significant fraction of those templates are not needed and can be removed from the template bank.

B. α_B-dependence

The moments used to estimate the metric components strongly depend on the parameter α. We refer to this parameter as α_B to differentiate from the α parameter (or equivalently from α_F) that is used in the filtering process. As shown in figure 1, the number of templates changes significantly when α_B varies. There is a drop in the number of templates around $\alpha_B = 10^{-2}$. We want to minimize the template bank size but we also need to consider the *efficiency* of the bank as defined in [14, 15], and choose α_B appropriately. Indeed, we expect the efficiency of the template bank to be also affected by this parameter. We performed simulated injections so as to test the efficiency of the template bank for various values of α_B. Results are summarized in figure 2 for three typical values of α_B. Because efficiencies are very similar, we decided to use an α_B parameter such that the number of templates is close to a minima, that is 10^{-2}. In all the following simulations and LIGO searches, $\alpha_B = 10^{-2}$.

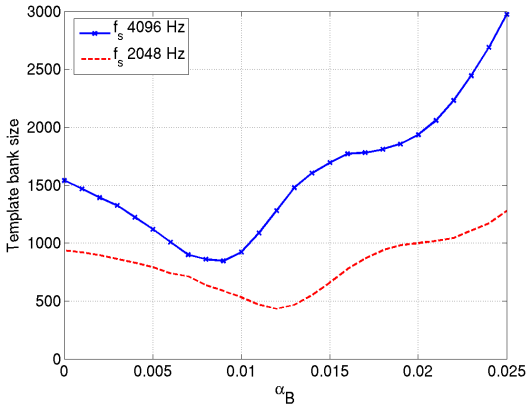

FIG. 1: The size of the template bank function of the α_B. The two curves show the template bank size versus α_B parameter for two values of sampling frequency. The two curves show the same pattern with a drop around $\alpha_B = 10^{-2}$, where template bank sizes are twice as low as compared to $\alpha_B = 0$ or $\alpha_B = 2.5\,10^{-2}$. This evolution of the template bank size is directly linked to the moment computation (see equation A6), where the parameter α_B is used. Efficiency of a template bank is not strongly related to this parameter (see figure 2) so we choose a value that corresponds to the smallest bank size. In real analysis, we use 2048 Hz and for simplicity a value of $\alpha_B = 10^{-2}$ was chosen. In this example, we used the same simulation parameters as in Sec. IV A.

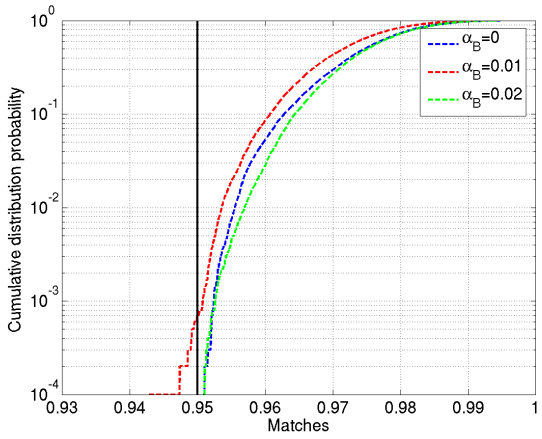

FIG. 2: Template bank efficiencies versus α_B parameter. The α_B parameter does not significantly affect the matches. Most of them are above the minimal match of 95%, and more importantly the three distributions are close to each other. In this example, we used the same simulation parameters as in Sec. IV A, and EOB injections.

C. Template Bank using ending frequency layers

Starting from each template that is placed in the ψ_0–ψ_3 plane, we need to lay templates along the third dimension, which is the ending cut-off frequency $f_{\rm cut}$ of the template. Because the mismatch is first order in $\Delta f_{\rm cut}$

[8], it cannot be described by a metric.

Using an exact formula, Ref. [8] proposed to lay templates with different $f_{\rm cut}$ values between $f_{\rm min}$ and $f_{\rm end} = f_{\rm Nyquist}$ that depend on the region searched for. We populate the $f_{\rm cut}$ dimension as follows. First, we estimate the frequency of the last stable orbit which we refer to as $f_{\rm min}$, and the frequency at the light ring which we refer to as $f_{\rm max}$. Between $f_{\rm min}$ and $f_{\rm max}$, we place $N_{\rm cut}$ layers of templates with the ending frequency chosen at equal distance between $f_{\rm min}$ and $f_{\rm max}$. The frequency at the last stable orbit and light ring are defined in terms of the total mass ($f_{\rm min} = 1/M/\pi/6^{3/2}/$, $f_{\rm max} = 1/M/\pi/3^{3/2}$). The total mass is computed for each template using an empirical expression similar to equation 2.4: $M \approx -\psi_3/32/\pi^2/\psi_0$. Although this expression is an approximation, the resulting template bank gives high match with various physical template families as shown in Sec. IV. In all our simulations and searches, we set the minimal match (MM) [12] to 95%, so there is no guarantee that the relation between M and $\psi_{0,3}$ is suitable for minimal matches far from 95%.

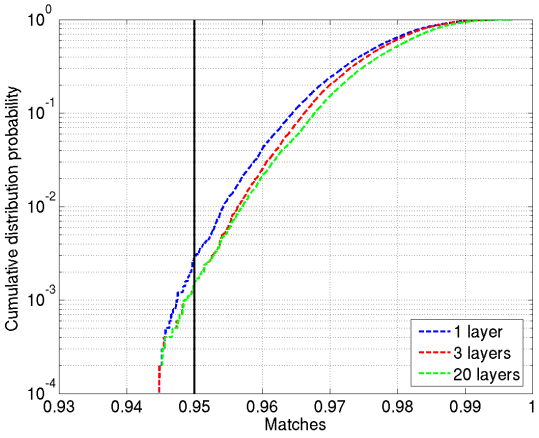

FIG. 3: Template bank efficiencies versus number of layers, $N_{\rm cut}$, in the $f_{\rm cut}$ dimension. With the current template bank design, $N_{\rm cut}$ does not affect the matches significantly. The cumulative distribution of matches over 10,000 simulations shows only small differences between 3 and 20 layers. Even the results obtained with 1 layer are not that far from $N_{\rm cut} = 3$. In our real analysis and simulations, we used $N_{\rm cut} = 3$. In this example, we used the same simulation parameters as in Sec. IV A, and EOB simulated injections.

D. Polygon Fit

The boundaries of the template bank are defined by the ranges of the parameters ψ_i and the span of the cut-off frequency $f_{\rm cut}$ in such a way that BBH systems with component mass as low as 3 $M_\odot$ are detectable. The ψ_i ranges provided in Sec. III A cover a squared area that is actually too wide: a significant fraction of the templates are not targetting the BBH systems we are searching for. Therefore, in order to reduce the template bank size and optimize our searches, we introduce an extra procedure that selects the pertinent templates only. This procedure is known as a *polygon fit* and works as follows. First, we create a BCV template bank with the range of ψ_0 and ψ_3 parameters as large as possible, and for our purpose, as quoted in Sec. III A. This choice of ranges allows to detect BBH systems but also black hole - neutron star (BHNS) systems. Since, we focus on the BBH systems only, we perform many BBH simulated injections and filter them with the template bank that has been created. For each injection, we keep the ψ_0 and ψ_3 parameters of the template that gives the best match. We gather all the final pairs of ψ_0, ψ_3 parameters, and superposed them on top of the original template bank. It appears that only about a third of the templates are required to detect BBH systems with a high match. This sub-set of templates can be used to define a polygon area that enclose all of them. The resulting polygon area defines the boundaries of our new template bank and results in a template bank three times smaller than the original one.

In figure 4, we show such a template bank that is within the boundary of a polygon constructed with our simulated injections. The coordinates of this polygon are chosen empirically. For safety, the boundaries are chosen loosely, therefore the template bank has also the ability to detect non-spinning BHNS. It is worth noticing that with this template bank designed to detect BBH many BHNS systems are found with a match greater than the requested MM (See Sec. IV C).

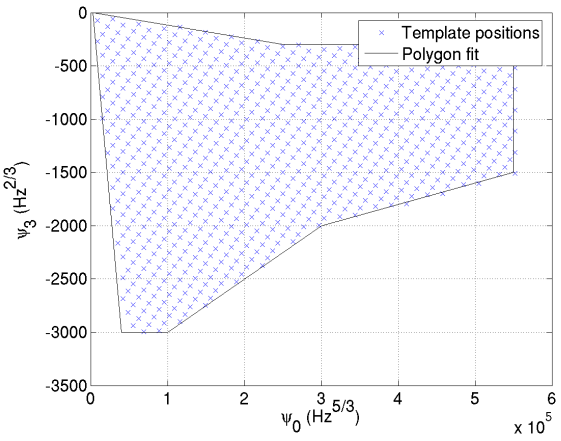

FIG. 4: Example of parameter space and template bank placement. This plot shows a projection of the templates onto the ψ_0/ψ_3 plane. Simulations and equation 2.4 gives an estimation of the mapping between the phenomenological parameters and the chirp mass of the simulated injections. Low mass systems such as a $(3,3)M_\odot$ are in the RHS, high mass systems lie on the LHS and asymmetric systems in the bottom left corner. In this example, we used the same parameters as in Sec. IV B.

IV. SIMULATIONS

In the following simulations, we fix the sampling frequency to 2048 Hz, $\alpha_B = 10^{-2}$, $N_{\rm cut} = 3$, the ψ_0 and ψ_3 ranges are provided in Sec. III A and a polygon fit as in figure 4 is used. The simulated injections are based on several physical template families that are labelled EOB, PadeT1, TaylorT1, and TaylorT3 [17–21] with the phase expressed at 2PN order (see [15] for more details). The population of simulated injections has a uniform total mass. Although this choice is not based on any astronomical observation, it is convenient to estimate the efficiency of our template banks. We use a noise model that mimics the design sensitivity curve of initial LIGO (see [9, 15]), and the minimal match is $MM = 95\%$. We performed 2 simulations that are closely related to the third and fourth LIGO science run's BBH searches [3].

A. Example 1

The first set of simulations uses a lower cut-off frequency of 70 Hz, as in S3 BBH search [3]. The largest component mass and the total mass of the simulated injections are set to 40 $M_\odot$. The template bank has 531 templates. The results are summarized in figure 5 which shows the efficiency of the template bank versus the total mass. There are a few injections found with a match as low as 93% for total mass $M < 6.5\ M_\odot$. Closer inspection shows that several issues are linked to this feature. First, we used a sampling frequency of 2048 Hz, which reduces the template bank size by $\approx 50\%$ as compared to a sampling of 4096 Hz. Second, we set $\alpha_B = 10^{-2}$, which reduces the template bank size by $\approx 50\%$ as compared to $\alpha_B = 0$. Finally, the number of layers, $N_{\rm cut}$, is limited to 3. Therefore, this tuning significantly reduced the template bank size with the cost of losing about only 1 to 2% SNR for a small fraction of the parameter space considered. From $M = 6.5\ M_\odot$ to about $M = 20\ M_\odot$, matches are above 95%. In the high mass range, a large fraction of the simulated injections are found below the minimal match (but larger than 90%): 20% in the case of TaylorT1, TaylorT3, and PadeT1 models, and only 0.1% in the case of EOB injections. This effect is expected because the lower cut-off frequency is high, and therefore many of the high mass systems considered are very short (i.e., less than 100 ms).

B. Example 2

The second set of simulations uses a lower cut-off frequency of 50 Hz, as in S4 BBH search [3]. The largest component mass and the total mass of the simulated injections are set to 80 $M_\odot$. The template bank has 1609 templates. The results are summarized in figure 6. Up to $M \approx 40\ M_\odot$, most of the injected simulations are recovered with matches above 95%. However, a small fraction

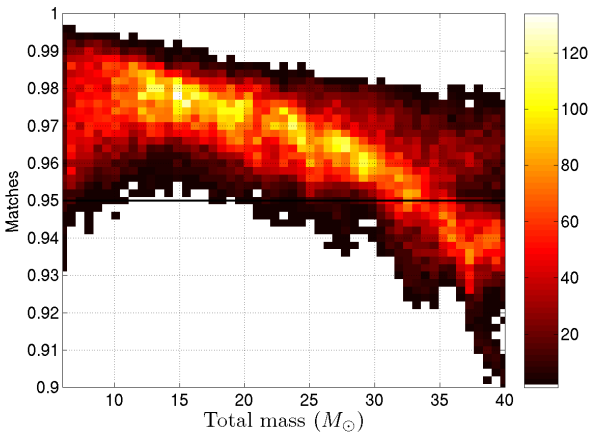

FIG. 5: Distribution of the efficiency versus the total mass. The simulation consisted of $N_s = 40,000$ injections. The lower cut-off frequency for the injections and the BCV templates was set to 70 Hz, as in S3 BBH search.

is found with matches below 95%, which represent 0.1% of the EOB, PadeT1, and TaylorT1 injections, and 3% of the TaylorT3 injections. In the high mass region (up to 60 $M_\odot$), 20% of the injections are below the required minimal match for the TaylorT1, TaylorT3, and PadeT1 injections, and only 0.5% of the EOB injections. If we consider injections with total mass from 60 to 80 $M_\odot$, almost 10% of EOB are below the minimal match (but above 92%). As for other models, matches drop quickly towards zero down to 40%, which is due to shorter and shorter duration of the injected waveforms.

C. Example 3

As stated in Sec. III D, although the template bank is designed to target BBH systems, it has the ability to detect some BHNS systems as well. The goal of this third simulation is to demonstrate that indeed many BHNS systems are detectable with a high match by using the template designed to search for BBH systems in S3 and S4 data sets.

The parameters used are exactly the same as in the second example. The largest component mass and the total mass of the simulated injections are set to 80 $M_\odot$. The lowest component mass is 1 $M_\odot$, and we impose the systems to be BHNS only (the mass of the neutron star is less than 3 $M_\odot$, and the mass of the black hole is larger than 3 $M_\odot$). The template bank is identical to the second simulation (1609 templates). The results are summarize in figure 7, where we plot matches as a function of the two component masses. We found that 60% of the BHNS injections are recovered with the match larger than 95%, 77% with the match larger than 90%, and 98% with the match greater than 50%. Therefore, using the same bank as in S3 and S4 searches, whose boundaries resulting from

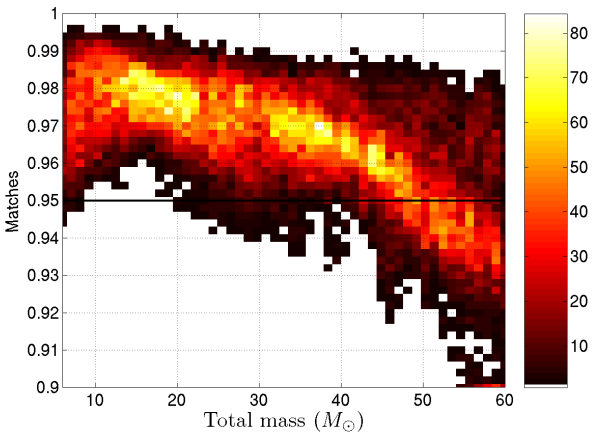

FIG. 6: Distribution of the efficiency versus the total mass. The simulation consisted in $N_s = 40,000$ injections. The lower cut-off frequency of the injections and the BCV templates is 50 Hz, as in S4 BBH search. For convenience (same scale as in figure 5), we do not show simulated injections with total mass above 60 $M_\odot$ and matches below 90%. Matches of the injections with the total mass greater than 60 solar mass can drop significantly below the minimal match for symmetric systems: 20% of the injections are below the minimal match for the TaylorT1, TaylorT3, and PadeT1 injections (only 0.5% of the EOB injections are below 95%).

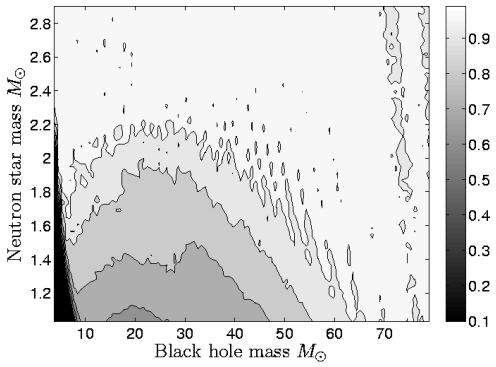

FIG. 7: Matches between the BCV template bank used to search for BBH systems and BHNS injections. 77% of the BHNS injections are found with a match larger than 90%. See the text for more details.

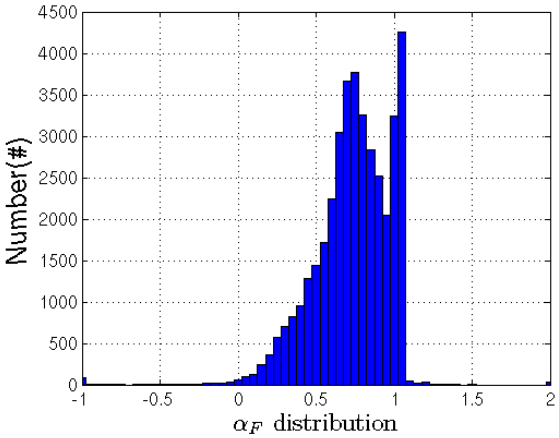

FIG. 8: Distribution of the α_F parameter corresponding to simulations made in Sec. IV B. Most of the found simulated injections have an α_F value between zero and unity. However, a significant fraction are distributed around $\alpha_F = 1$. Those triggers correspond to $M > 60\ M_\odot$, for which waveforms cannot be differentiated from a transient noise (short duration).

the polygon fit were deliberately chosen to be slightly wider than necessary, we can detect a significant fraction of the BHNS systems. It is also clear from the figure that the lightest systems have a very low match. This was expected since the template bank aimed at detecting systems whose total mass is greater than $6M_\odot$, as defined by the maximum of the ψ_0 range.

We performed a second test where the polygon fit is not applied anymore. The template bank is then much larger with 4635 templates but we found that 78% of the BHNS injections are recovered with a match larger than 95%, 94% with a match larger than 90%, and 98% with a match greater than 50%. The size of such a template bank is comparable to a template bank that uses physical template families (e.g., with the same parameter as above, a hexagonal placement for physical template families [15] that covers a parameter space from 1 to 80 solar mass has about 3000 templates if we exclude the templates for which both component mass are below 3 $M_\odot$).

The events which are found with a low match (say, 60% or lower) correspond to low mass systems where the neutron star's mass is less than 2.5 $M_\odot$ and the BH's mass less than 7 $M_\odot$ which can be taken care of by increasing the range of ψ_0.

D. Discusions

In this section, we would like to check that (i) the triggers related to the injections have $0 \leq \alpha_F \leq 1$, and (ii) the range of validity of equation 2.4 that gives an estimation of the chirp mass.

We use the results of the simulations performed in the example 2. First, we plot an histogram of all the α_F values that correspond to the 40,000 simulated injections. Although we impose α_F to be in the range $[0, 1]$, we keep track of the SNR expression that was used, namely, in which regime of α_F we were. The population above 60 $M_\odot$ tends to have α_F values closer to 1. However, most of the systems with $M < 60\ M_\odot$ have $0 < \alpha_F < 1$ so the constrained SNR is equivalent to the unconstrained SNR as stated in Sec. II.

In Fig 9, we plot the errors on the chirp mass (i.e., $(\mathcal{M}_i - \mathcal{M}_e)/\mathcal{M}_i$, where i stands for injected, and e for estimated). The errors are within 10% for BBH systems

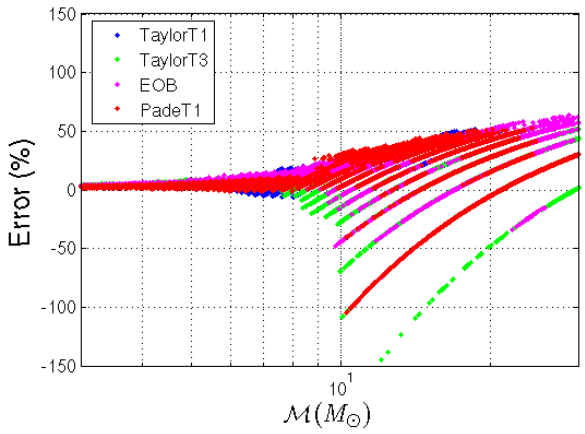

FIG. 9: Errors in chirp mass estimation corresponding to simulations made in Sec. IV B. Errors increase significantly for $\mathcal{M}$ greater than 8 solar mass with errors larger than 50%.

when the chirp mass is below $\approx 8\ M_\odot$. However, errors increase significantly when $\mathcal{M} \gtrsim 8\ M_\odot$ because (i) parameter estimation of high mass BBH systems is intrinsically weak, even for physical template families and (ii) BCV templates are known to be detection template families that are not suitable for parameter estimation.

V. CONCLUSIONS

The BCV template bank that we described in this paper was used to search for BBH systems in the S2, S3 and S4 LIGO data sets. We described the significant improvements that were made between the S2 search and the S3/S4 searches: α_B tuning, hexagonal lattice, and polygon fit. These improvements reduce the template bank size by an order of magnitude, while keeping the efficiency higher than 95% for most of the BBH systems considered. Consequently, despite lower cut-off frequency which was reduced from 100 Hz to 50 Hz between the second and the fourth science runs, the template bank size remained similar.

A principal motivation for the construction of a detection template bank was to use a single template bank instead of several physical template families. The template bank size is therefore an important aspect of a BCV search, and we have shown in this work how the number of templates can be optimized to search for BBH. Remarkably, the same template bank has a high match with a wide range of BHNS.

More importantly, the BCV template bank was designed to search for BBH systems in the context of S2 LIGO search. That is, for a lower cut-off frequency of 100 Hz for which most of the target waveforms are short duration waveforms. However, LIGO detectors improved and are still improving at low frequency, making the waveforms longer. The advantage of using a BCV template to search for systems as low as 3 $M_\odot$ is no longer evident, especially considering the absence of a well defined χ^2 test for phenomenological templates. Therefore if it were to be used, the author thinks that a BCV template bank should be used to search for a mass range starting at a higher value, such as 10, 20 $M_\odot$.

Acknowledgments

We would like to acknowledge many useful discussions with members of the LIGO Scientific Collaboration inspiral analysis group which were critical in the formulation of the results described in this paper. This work has been supported in part by Particle Physics and Astronomy Research Council, UK, grant PP/B500731. This paper has LIGO Document Number LIGO-P070089-00-Z.

APPENDIX A: METRIC

We can derive an expression for the match between two BCV templates (described by Eq 2.3, 2.1 and 2.2). First, we consider templates with the same amplitude function (i.e., the same α and $f_{\rm cut}$ parameter). The overlap $\langle h(\psi_0,\psi_3), h(\psi_0+\Delta\psi_0,\psi_3+\Delta\psi_3)\rangle$ between templates with close values of ψ_0 and ψ_3 can be described (to second order in $\Delta\psi_0$ and $\Delta\psi_3$) by the mismatch metric g_{ij} [8]:

$$\langle h(\psi_0,\psi_3), h(\psi_0+\Delta\psi_0,\psi_3+\Delta\psi_3)\rangle = 1 - \sum_{i,j=0,3} g_{\rm ij}\,\Delta\psi_i\Delta\psi_j. \tag{A1}$$

The metric coefficients g_{ij} can be evaluated analytically [8], and are given by

$$g_{ij} = \frac{1}{2}\left[M_1 M_2^{-1} M_3\right], \tag{A2}$$

where the $\mathbf{M}_{(1)\ldots(3)}$ are the matrices

$$\mathbf{M}_{(1)} = \begin{bmatrix} J(2n_0) & J(n_0+n_{3/2}) \\ J(n_0+n_{3/2}) & J(2n_{3/2}) \end{bmatrix}, \tag{A3}$$

$$\mathbf{M}_{(2)} = \begin{bmatrix} J(n_0) & J(n_{3/2}) \\ J(n_0-1) & J(n_{3/2}-1) \end{bmatrix}, \tag{A4}$$

$$\mathbf{M}_{(3)} = \begin{bmatrix} J(0) & J(-1) \\ J(-1) & J(-2) \end{bmatrix}, \tag{A5}$$

and where

$$J(n) \equiv \left[\int \frac{|\mathcal{A}(f)|^2}{S_h(f)} \frac{1}{f^n} df\right] \Big/ \left[\int \frac{|\mathcal{A}(f)|^2}{S_h(f)} df\right]. \quad \text{(A6)}$$

Let us emphasize the fact that the mismatch $\langle h(\psi_0, \psi_3), h(\psi_0 + \Delta\psi_0, \psi_3 + \Delta\psi_3)\rangle$ is translationally invariant in the ψ_0–ψ_3 plane, so the metric g_{ij} is constant everywhere since $J(n)$ is independent of ψ_0, ψ_3 parameters.

APPENDIX B: FILTERING AND α-MAXIMIZATION

1. Filtering

The BCV templates in the frequency domain are defined by equation 2.1. The amplitude part of a BCV template $\mathcal{A}(f)$ can be decomposed into linear combinations of $f^{-7/6}$ and $f^{-1/2}$. These expressions can be used to construct an orthonormal basis $\{\hat{h}_k\}_{k=1..4}$. We want the basis vectors to satisfy

$$\left\langle \hat{h}_i, \hat{h}_j \right\rangle = \delta_{ij}. \quad \text{(B1)}$$

First, we construct two real functions $\mathcal{A}_1(f)$ and $\mathcal{A}_2(f)$ that satisfy $\langle A_i, A_j\rangle = \delta_{ij}$. Then, by defining $\hat{h}_{1,2}(f) = \mathcal{A}_{1,2}(f)e^{i\phi}, \hat{h}_{3,4}(f) = i\mathcal{A}_{1,2}(f)e^{i\phi}$ which will give $\left\langle \hat{h}_i, \hat{h}_j \right\rangle = \delta_{ij}$, and the desired basis, $\{\hat{h}_k\}$. We can choose the following basis functions

$$\begin{bmatrix} \mathcal{A}_1(f) \\ \mathcal{A}_2(f) \end{bmatrix} = \begin{bmatrix} a_{11} & 0 \\ a_{21} & a_{22} \end{bmatrix} \begin{bmatrix} f^{-7/6} \\ f^{-1/2} \end{bmatrix}, \quad \text{(B2)}$$

where the normalization factor are given by

$$a_1 = I_{7/3}^{-1/2}, b_1 = -\frac{I_{5/3}}{I_{7/3}} \left(I_1 - \frac{I_{5/3}^2}{I_{7/3}}\right)^{-1/2}, \quad \text{(B3)}$$

$$\text{and } b_2 = \left(I_1 - \frac{I_{5/3}^2}{I_{7/3}}\right)^{-1/2}, \quad \text{(B4)}$$

and the integrals I_k are defined by

$$I_k = 4\int_0^{f_{\rm cut}} \frac{f^{-k}}{S_h(f)} df. \quad \text{(B5)}$$

The normalized template can be parametrized using two angles, the orbital phase ϕ and an angle ω

$$\begin{aligned} \hat{h}(\theta, \omega; f) \;=\; & \quad \text{(B6)} \\ & \hat{h}_1(f)\cos\omega\cos\phi_0 + \hat{h}_2(f)\sin\omega\cos\phi_0 \\ & + \; \hat{h}_3(f)\cos\omega\sin\phi_0 + \hat{h}_4(f)\sin\omega\sin\phi_0 \end{aligned}$$

where w is related to α by (see [6])

$$\tan\omega = -\frac{a_1\alpha}{b_2 + b_1\alpha}. \quad \text{(B7)}$$

It follows that for any given signal s, the overlap is

$$\begin{aligned} \rho \;&=\; \left\langle s|\hat{h}\right\rangle \quad \text{(B8)} \\ &=\; x_1\cos\omega\cos\phi_0 + x_2\sin\omega\cos\phi_0 \\ &+\; x_3\cos\omega\sin\phi_0 + x_4\sin\omega\sin\phi_0, \end{aligned}$$

where $x_i = \langle s|h_i\rangle$. We can then maximized over ω (i.e., α), and ϕ_0 without any constraint on the α parameter, which leads to the unconstrained SNR given by

$$\rho_U = \frac{1}{\sqrt{2}}\sqrt{\left(V_0 + \sqrt{V_1^2 + V_2^2}\right)} \quad \text{(B9)}$$

where

$$\begin{aligned} V_0 \;&=\; x_1^2 + x_2^2 + x_3^2 + x_4^2, & \text{(B10)} \\ V_1 \;&=\; x_1^2 + x_3^2 - x_2^2 - x_4^2, & \text{(B11)} \\ V_2 \;&=\; 2(x_1x_2 + x_3x_4). & \text{(B12)} \end{aligned}$$

2. α-maximization

Starting from equation B8, we can derive a constrained SNR ρ_C that depends upon the value of the parameter α_F. Therefore, we need to maximize equation B8 over the parameter ϕ_0 only. This maximization gives

$$\rho(\omega) = \max_{\omega} \frac{1}{\sqrt{2}}\sqrt{V_0 + V_1\cos 2\omega + V_2\sin 2\omega}. \quad \text{(B13)}$$

If $\alpha_F < 0$, we want to use a SNR calculation for which $\omega = 0$, which means $\alpha_F = \alpha = 0$. Therefore, the constrained SNR is

$$\rho_C^0 = \frac{1}{\sqrt{2}}\sqrt{V_0 + V_1}. \quad \text{(B14)}$$

If $\alpha_F > 1$, we want to use a SNR calculation for which $\omega = \omega_{\rm max}$, which means that $\alpha_F = 1$ (i.e., $\alpha = f_{\rm cut}^{-2/3}$), and the angle $\omega = \omega_{\rm max}$ is then a maxima that is given by

$$\omega_{\rm max} = \arctan\left\{-\frac{a_1 f^{-2/3}}{b_2 + b_1 f^{-2/3}}\right\}. \quad \text{(B15)}$$

The constrained SNR is then given by

$$\rho_C^1 = \frac{1}{\sqrt{2}}\sqrt{V_0 + V_1\cos 2\omega_{\rm max} + V_2\sin 2\omega_{\rm max}}. \quad \text{(B16)}$$

Finally, using the relation $V_1\cos 2\omega + V_2\sin 2\omega = \sqrt{V_1^2 + V_2^2}\cos(2\omega - \theta)$, where $\tan\theta = V_2/V_1$, we can rewrite equation B13 in the general case where $0 < \alpha_F < 1$ by imposing $2\omega = \theta$, which gives

$$\rho_C = \frac{1}{\sqrt{2}}\sqrt{\left(V_0 + \sqrt{V_1^2 + V_2^2}\right)}, \quad \text{(B17)}$$

that is an identical expresion as in equation B9 (i.e., $\rho_C = \rho_U$). More details on this derivation can be found in [22].

[1] A. Abramovici *et al.* 1992 *Science* **256**, 325 ; B. Abbott, *et al.* 2004 *Nuclear Inst. and Methods in Physics Research*, A **517/1-3** 154

[2] B. Abbott *et al.* 2005 LIGO Scientific Collaboration, *Phys. Rev.* D **72** 082002, gr-qc/0505042

[3] B. Abbott *et al.* 2007 LIGO Scientific Collaboration, arXiv:0704.3368 [gr-qc]

[4] B. Abbott *et al.* 2004 LIGO Scientific Collaboration, *Phys. Rev.* D **69** 122001, gr-qc/0308069

[5] B. Abbott *et al.* 2005 LIGO Scientific Collaboration, *Phys. Rev.* D **72** 082001, gr-qc/0505041

[6] B. Abbott *et al.* 2006 LIGO Scientific Collaboration, *Phys. Rev.* D **73** 062001, gr-qc/062001

[7] L. Blanchet 2003 *Living Rev. Rel.* **5**, gr-qc/0202016

[8] A. Buonanno, Y. Chen and M. Vallisneri, *Phys. Rev.* D **67** 024016, gr-qc/0205122

[9] R. Balasubramanian, B.S. Sathyaprakash, S.V. Dhurandhar 1996 *Phys. Rev.* D **53** 3033 ; Erratum-ibid. D **54**, 1860

[10] B.S. Sathyaprakash and S.V. Dhurandhar 1991 *Phys. Rev.* D **44**, 3819

[11] F. Beauville *et al.* 2005 *Class. Quant. Grav.* **22**, 4285

[12] B. Owen 1996 *Phys. Rev.* D**53**, 6749

[13] B. Owen, B. S. Sathyaprakash 1998 *Phys. Rev.* D **60** 022002

[14] S. Babak and R. Balasubramanian and D. Churches and T. Cokelaer and B. S. Sathyaprakash 2006 *Class. Quant. Grav.* **23**, 5477

[15] T. Cokelaer 2007 *Gravitational Wave Detections of Inspiralling Compact Binaries: Hexagonal Template Placement and Physical Template Families*, gr-qc/arXiv:0706.4437v1

[16] R. Prix, *Template-based searches for gravitational waves:efficient lattice covering of flat parameter spaces* LIGO document P070030-01-Z-1

[17] L. Blanchet, B. R. Iyer, C. Will and A. Wiseman 1996 *Class. Quant. Grav.* **13** 575

[18] T. Damour, B. R. Iyer and B. S. Sathyaprakash 1998 *Phys. Rev.* D **57** 885

[19] A. Buonanno and T. Damour 1999 *Phys. Rev.* D **59** 084006

[20] A. Buonanno and T. Damour 2000 *Phys. Rev.* D **62** 064015

[21] T. Damour, P. Jaranowski and G. Schäfer 2000 *Phys. Rev.* D **62** 084011

[22] A. Buonanno, Y. Chen, M. Vallisneri, Using *Alpha as Extrinsic Parameter in the template family*, LIGO document T050170-00.pdf, url=http://www.ligo.caltech.edu/docs/T050170-00.pdf